



PAPER

Design principles for $>90\%$ efficiency and $>99\%$ indistinguishability broadband quantum dot cavities

OPEN ACCESS

RECEIVED

16 May 2024

REVISED

23 August 2024

ACCEPTED FOR PUBLICATION


2 September 2024

PUBLISHED

13 September 2024

Original Content from
this work may be used
under the terms of the
[Creative Commons
Attribution 4.0 licence](#).

Any further distribution
of this work must
maintain attribution to
the author(s) and the title
of the work, journal
citation and DOI.

D Dlaka^{1,*} , P Androvitsaneas^{1,2}, A Young¹, Q Ma¹, E Harbord¹ and Ruth Oulton¹¹ Quantum Engineering Technology Labs, H. H. Wills Physics Laboratory and Department of Electrical and Electronic Engineering, University of Bristol, Bristol, BS8 1FD, United Kingdom² School of Engineering, Queen's Buildings, Cardiff University, Cardiff CF24 3AA, United Kingdom

* Author to whom any correspondence should be addressed.

E-mail: david.dlaka@bristol.ac.uk**Keywords:** quantum dot, micropillar, cavity quantum electrodynamics, single photon sources, Purcell effect, solid state emitters**Abstract**

Quantum dots have the potential to be one of the brightest deterministic single photon sources with high end applications in quantum computing and cluster state generation. In this work, we re-examine the design of plain micropillars by meticulously examining the structural effects of the decay into leaky channels beyond an atom-like cavity estimation. We show that precise control of the side losses with the diameter and avoidance of propagating Bloch modes in the distributed Bragg reflectors can result in easy-to-manufacture broadband ($Q \approx 750\text{--}2500$) micropillars, allowing for broad optical coherent control pulses necessary for high single photon purity ($>99.2\%\text{--}99.99\%$ achievable) while simultaneously demonstrating extremely high efficiency out the top ($90.5\%\text{--}96.4\%$). We also demonstrate that such cavities naturally decouple from the phonon sideband, with the phonon sideband reducing by a factor of 5–33 allowing us to predict that the photons should show 98.5%–99.8% indistinguishability without the need for filtering.

1. Introduction

Highly efficient sources of quantum light—single and entangled photons—that are readily mass manufactured, are vital for quantum technologies and quantum communications. Quantum dots (QDs) have near unity internal quantum efficiency and their utility extends well past single- or pair- photon sources as they can be used as light-matter interfaces with a possible perfect non-linearity, which requires a simultaneous near-perfect indistinguishability and efficiency. To meet these requirements, one exploits cavity quantum electrodynamics (cQED) to create photonic structures, such as a micropillar cavity, which efficiently funnels the light into a single well-defined optical mode. The micropillar single photon source (SPS) consists of a QD placed inside a resonator made up of a λ/n ‘cavity’ layer and a quarter wavelength distributed Bragg reflector (DBR) stack on either end of the cavity. The resulting emitter-cavity interaction results in enhancement of emission along the growth axis, and by etching the sides of the planar structure into cylindrical micropillars, the field at the dielectric interfaces is laterally confined therefore reducing the resonator leakage through the sides and increasing decay into favourable channels.

Research into solid state single photon devices has produced very promising micropillar-QD emitters. The true potential of any cavity-enhanced SPS only occurs if the QD and cavity are degenerate, leading to various techniques being used to bring the QD energy into resonance with the cavity. Notably efficient devices had been experimentally realised with a variety of QD-tuning techniques, such as Stark-shifted QDs showing 65% efficient resonance fluorescence in high Q (12 000) pillars [1]. Similar work in spectrally narrow cavities showed $\approx 66\%$ collection into $NA = 0.65$ with simultaneously high single-photon purity and indistinguishability [2]. Further experimental demonstrations of bright micropillars were reported with $74.4 \pm 4\%$ overall efficiency in the near-IR [3]. More recently, novel approaches such as planar (non-etched) half-cavities with a microlens mirror completing the resonator achieved 57% end-to-end efficiency through a single mode fiber [4].

A common drawback most current state-of-the-art micropillar devices share is the reliance on strong Purcell enhancement which is achieved by resorting to narrow-band resonators, with Q factors >10000 and resulting cavity linewidths <0.1 meV. These are all too spectrally narrow to accommodate the short optical pulses (1–2 ps) required to avoid multiple excitation-relaxation cycles which are catastrophic to the single photon purity [5]. High Q factor pillars are extremely sensitive to the lifting of degeneracy in the emitter-resonator system, leading to a particular vulnerability to fabrication tolerances where asymmetry in the cylinder (ellipticity) causes the resonator to split into two non-degenerate H and V Γ_{Cavity} modes. On the other hand, broader cavities would be much more resistant to these and other fabrication tolerances, such as sidewall roughness, though techniques such as optical projection lithography can be used to fabricate micropillars with sufficiently smooth sidewalls to maintain a high Q factor. There have been demonstrations of this even at very small diameters at much faster speeds than e-beam lithography etching of the same structures [6]. What's more, a low Q cavity will spectrally encapsulate a much higher number of the QDs in the broadly distributed ensemble, leading to much better fabrication success rates. With this in mind, broadband cavities—meaning cavities which can accommodate a biexciton-exciton cascade and allow for picosecond pump pulses—have attracted attention and research efforts have demonstrated that low Q cavities can facilitate deterministic light-matter interactions, the efficiency of which can be maximised by suppressing lossy modes [7–9].

Other designs include exotic micropillar variations such as nanotrumpets that have been lifted off and placed on gold mirrors, with a predicted 75% efficiency [10], or hourglass-like micropillars, reaching 97% theoretical efficiency, albeit in very narrow cavity ($Q > 30k$) [11, 12]. Other techniques to utilise micropillars as on-demand SPSs include the introduction of controlled ellipticity in the cylinder structure, where the break in the radial symmetry splits the cavity decay channel into non-degenerate modes allowing for the pumping into one and extraction from the other [4]. This removes the cross-polarisation collection limit of more rudimentary pumping techniques, with efficiencies as high as 60% in structures at $Q=4000$ [13] and potentially 89% for $Q=25000$ [14] reported. However, asymmetric cavity designs preclude the encoding polarisation information in the qubit.

Furthermore, as these proposals involve technically difficult and resource intensive fabrication, there is still the necessity of a more scalable answer to the solid state SPS problem. In this work, we return to the basic micropillar structure due to its comparatively simpler manufacturability and proven potential as an ideal deterministic and versatile SPS. By discussing phenomena which are common to any cavity, we present a universally applicable and simple design strategy to maximise the device efficiency, indistinguishability, and bandwidth by providing an in-depth analysis of the hitherto underexplored low Q micropillars. We also consider the suppression of the phonon-photon interactions, leading to a near elimination of the phonon sideband and very high expected indistinguishability without filtering.

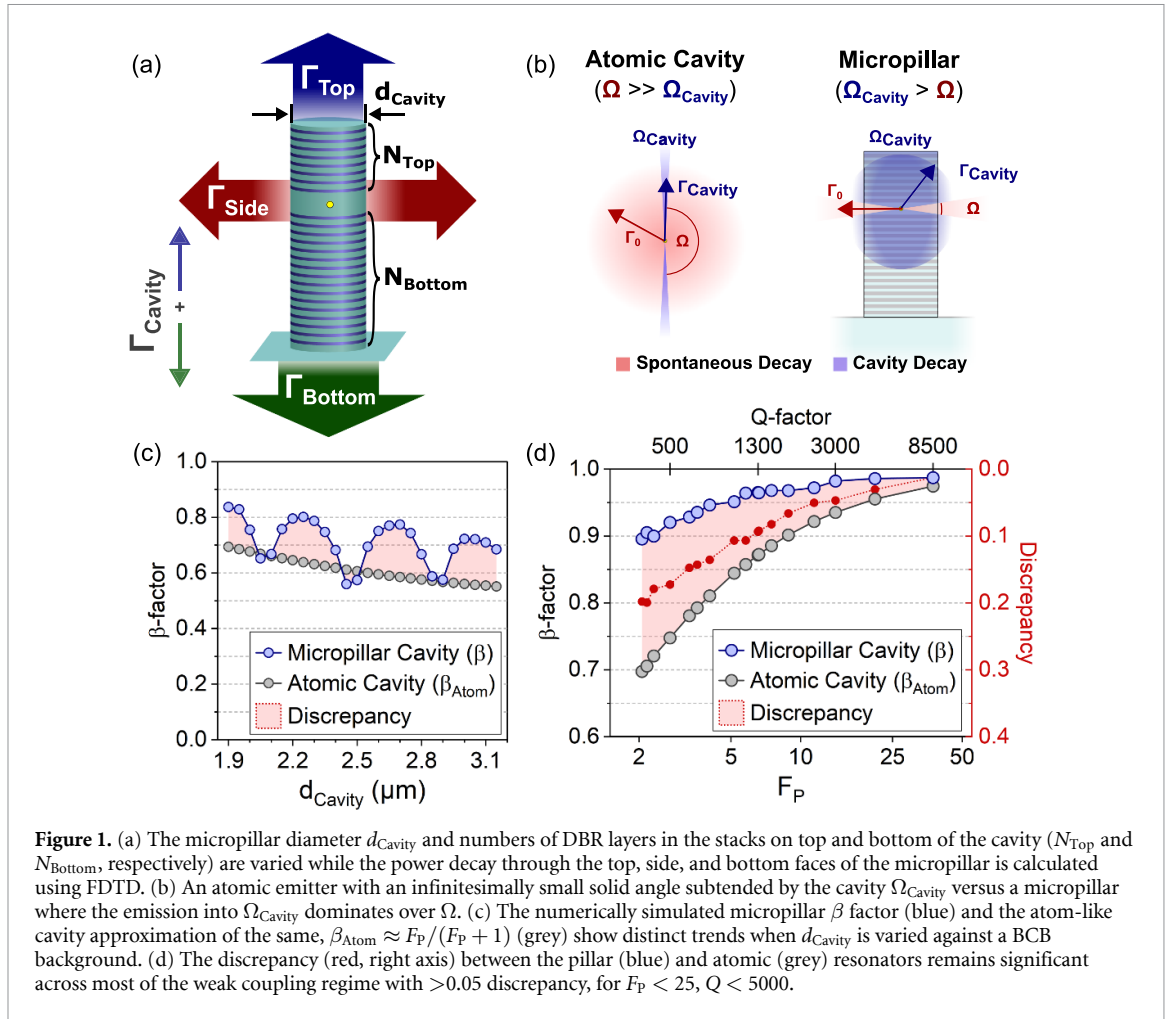
2. Methodology

We use a commercially available FDTD solver to fully examine the micropillar cQED by probing the diameter and DBR stack effects on the efficiency. We start off with a $d_{\text{Cavity}} = 2.25 \mu\text{m}$ ‘pilot’ pillar consisting of GaAs/AlAs DBRs with 7/35.5 pairs on the top/bottom respectively, and at the end we optimise to design high-brightness broadband pillars. The DBR layers are $\lambda/4n$, which for $n_{\text{GaAs}} = 3.41$ and $n_{\text{AlAs}} = 2.91$ corresponds to $d_{\text{GaAs}} = 95.3$ nm and $d_{\text{AlAs}} = 111$ nm, with $d_{\text{Cavity}} = 381$ nm. We use benzocyclobutene (BCB) as the surrounding medium for some simulations as indicated in the figure captions, as it is a commonly used material to planarize micropillars [15]. We examine all decay rates through the pillar faces while making no assumptions about the side leakage or the background decay rate (figure 1(a)), but relying on the fundamental relation

$$\Gamma_{\text{Cavity}} + \Gamma_{\text{Side}} = F_P \Gamma_0 \quad (1)$$

where Γ_{Cavity} is the decay rate into the cavity, Γ_{Side} is the decay rate into leaky side modes and F_P is the Purcell factor, describing the enhancement of the decay rate if the emitter was placed in bulk, Γ_0 . The motivation is to avoid making the common approximation used in atom-cavity physics that the solid angle subtended by the cavity Ω_{Cavity} is much smaller than Ω (as illustrated in figure 1(b)). In atom-cavity systems, the k-space subtended by Ω_{Cavity} is neglected and $\Omega \approx 4\pi^2$, leading to the commonly used expression to parameterise the active cavity efficiency, $\beta_{\text{Atom}} = F_P / (F_P + 1)$.

By introducing a finite radius, the semi-infinite GaAs subtended by Ω is replaced with the reflective radial edges which form a horizontal resonator, as discussed in detail in section 3. The decay rate of the corresponding k-vectors is therefore *not* Γ_0 , but Γ_{Side} instead. A cavity that subtends a finite solid angle can therefore exhibit off-resonant Purcell *suppression* [16], which can be a crucial tool in maximising the device



efficiency; in other words, a cavity which dominates the angular space demands less Purcell enhancement over the spontaneous decay to achieve high β factors. We account for this, as well as any waveguiding effects of the vertical DBR structure, by working out the β factor in a numerically exact way such that

$$\beta = \frac{\Gamma_{\text{Cavity}}}{\Gamma_{\text{Total}}} = \frac{\Gamma_{\text{Cavity}}}{\Gamma_{\text{Cavity}} + \Gamma_{\text{Side}}}. \quad (2)$$

This possibility is not captured by the Purcell factor based estimation β_{Atom} , as can be seen in figure 1(c) where the decay-based calculation of the pilot pillar β factor behaves very differently. Even at a fixed diameter (panel (d)), β_{Atom} underestimates the true active coupling throughout a significant range ($F_{\text{P}} \leq 50$, $Q \leq 8500$) of the Purcell regime; this discrepancy has been observed and modelled in both micropillars and microposts [9, 17, 18], showing that in radially terminated structures a more detailed model needs to be considered. For a full appreciation of the efficiency at the first lens ξ , we must also consider the passive efficiency η which quantifies the percentage of emission from the top versus leakage of the cavity mode into the substrate such that

$$\eta = \frac{\Gamma_{\text{Top}}}{\Gamma_{\text{Cavity}}} = \frac{\Gamma_{\text{Top}}}{\Gamma_{\text{Top}} + \Gamma_{\text{Bottom}}} \quad (3a)$$

$$\xi = \beta\eta = \frac{\Gamma_{\text{Top}}}{\Gamma_{\text{Total}}}. \quad (3b)$$

By varying the fundamental structural parameters of the pilot device, we identify several competing decay mechanisms in the micropillar and use this as a design guideline to produce an array of device designs. In this work we focus on 3D simulations of devices in the telecoms O-band, though analogous results observed for 910 nm micropillars indicate that our optimisation method may be applied to any wavelength.

3. Side-loss suppression

In figure 1(c), there is a clear oscillation of the β factor with diameter; we have observed this behaviour in previous FDTD simulations having found it to be in agreement with experimental measurements [9]. The same effect has also been observed with analytical examinations using the Fourier Modal Method [17], where a detailed treatment describes this periodicity as a result of guided modes along a fibre-like model of the pillar. We build on this work by implementing the numerical FDTD technique which does not require the simplification of the vertical DBR pillar structure, verifying the main result, but showing that there are discrepancies when the index of the surrounding medium is changed. We therefore present an alternative lateral 1D Fabry Perot model which allows for a simple yet effective design strategy depending solely on the desired pillar wavelength and the cavity semiconductor material.

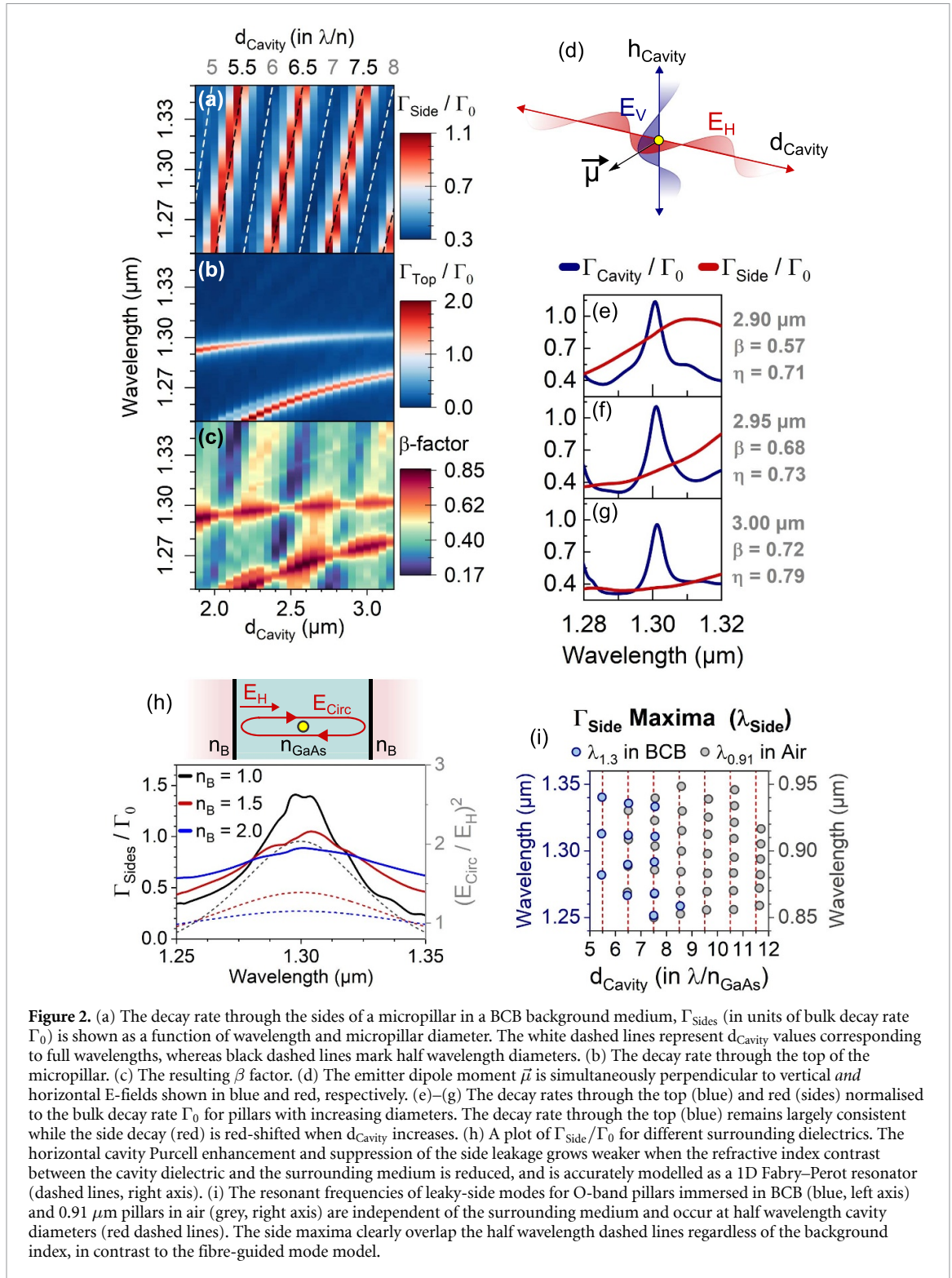
In figure 2(a) we calculate the power decay through the side, Γ_{Side} normalised to the decay rate in bulk GaAs, Γ_0 , as a function of wavelength and diameter d_{Cavity} . It can be seen that the strong horizontal leakage occurs at diameters corresponding to half wavelength values (black dashed lines) whereas at full wavelength diameters (white dashed lines), $\Gamma_{\text{Side}} \ll \Gamma_0$. The lossy Γ_{Side} can be suppressed from 1.1 to 0.3 Γ_0 ; as the fundamental cavity mode varies very little with diameter (figure 2(b)), the resulting active coupling to the cavity as described by (2) and presented in figure 2(c) shows regions of high β factor ($\approx 85\%$) separated by areas of much lower β ($\approx 55\%$) when the peaks in Γ_{Side} spectrally overlap the Γ_{Cavity} modes.

The diameter's effect on the side leakage is considerable as the etching introduces a reflective radial edge, resulting in a horizontal resonator formed by fields reflecting at the cavity-air boundary. The horizontal standing modes which are analogous to the vertical ones, result in distinct and separate horizontal modes in addition to the cavity modes. (figure 2(d)). When the diameter is changed, the resonant frequencies of the horizontal resonator are shifted much like the cavity height controls the resonances of the vertical modes. In figures 2(e)–(g), the cavity mode (blue) remains unperturbed by the small increments in the pillar diameter, while the much broader side mode (red) is shifted as the wider diameters means a longer horizontal cavity, and standing waves of a higher wavelength are resonant instead. While the side leakage is Purcell enhanced at wavelengths for which the horizontal cavity (pillar diameter) is resonant, we observe that Γ_{Side} is Purcell suppressed otherwise; by tuning the horizontally resonant frequencies away from the vertical cavity ones, we can use simultaneous Purcell enhancement of the cavity and Purcell suppression of the side channel at 1.3 μm to further increase β well past β_{Atom} because $\Gamma_{\text{Side}} \ll \Gamma_0$, causing β to increase from 57% to 72% as d_{Cavity} goes from 2.9 to 3 μm in figures 2(e)–(g) (the η factor also changes—this is discussed in section 4). This suppression is the crucial effect that is not captured by the atomic estimation and is responsible for the results in figures 1(c) and (d).

To further investigate the suitability of the 1D Fabry Perot model of the horizontal modes, we keep a constant pillar diameter and instead change the index of the background medium, n_B . In figure 2(h) we show a diagram of the input field E_H and the field reflected at the edge and circulating inside the resonator, E_{Circ} , as described by standard model in [19] where the resonator enhancement is given by

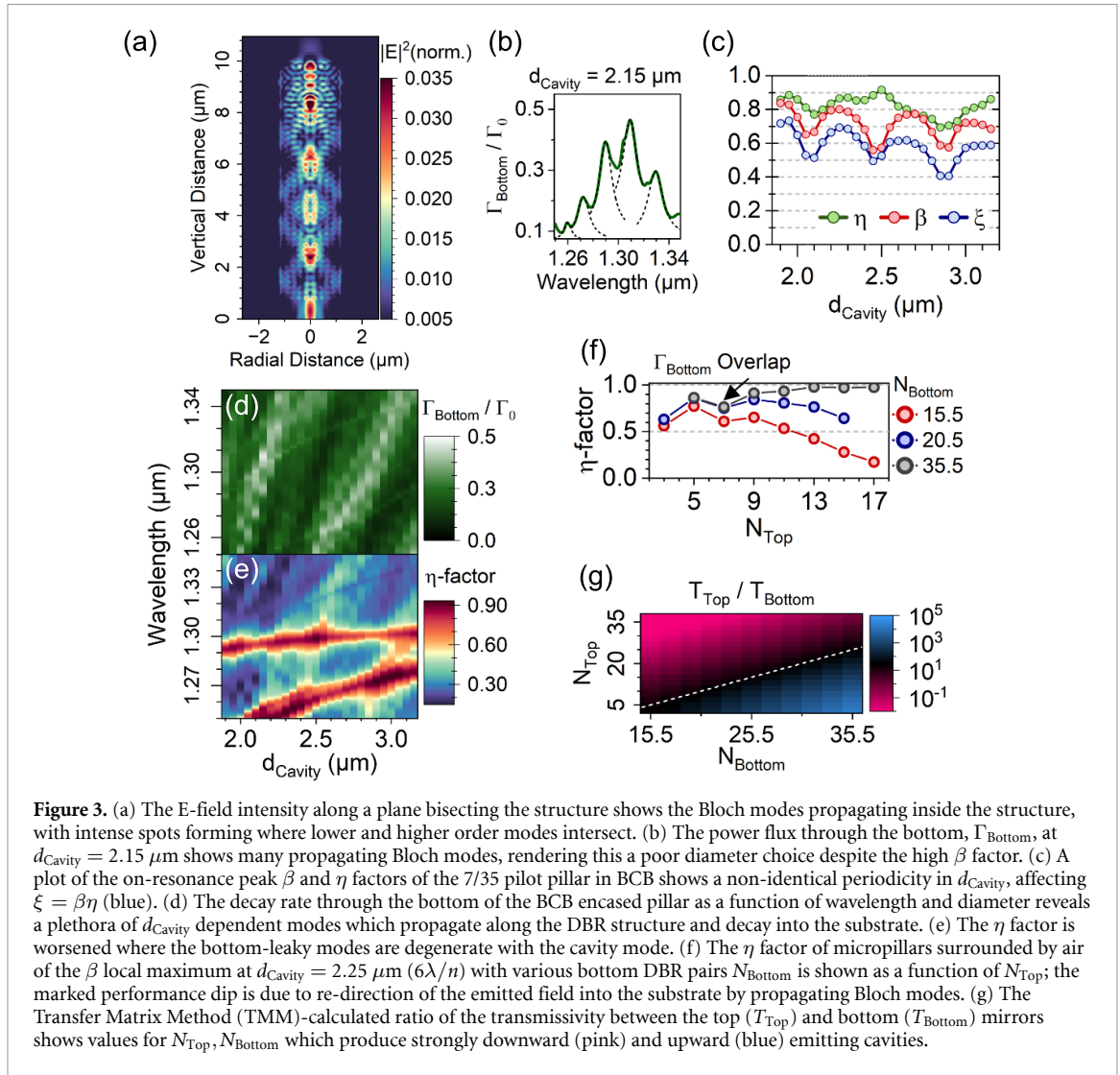
$$\frac{|E_{\text{Circ}}|^2}{|E_H|^2} = \frac{1}{(1-R)^2} \quad (4)$$

where R is the Fresnel coefficient given by $(n_{\text{GaAs}} - n_B)^2 / ((n_{\text{GaAs}} + n_B))^2$. The plot in figure 2(h) shows how Γ_{Side} is affected by the increase in n_B , whereas the dashed lines correspond to the right axis and show the resonator enhancement as predicted by (4). The decreasing contrast weakens the reflection at the radial boundary, reducing the wavelength variation of the Purcell effect (both on-resonant enhancement, and off-resonant suppression) of the side resonator, but does not otherwise affect their spectral position, in contrast to the fibre-guided mode model. This allows us to optimise the diameter using solely the desired micropillar wavelength and the material of the cavity layer i.e. for optimal β factors, $d_{\text{Cavity}} = m\lambda/n_{\text{Cavity}}$ where $m \in \mathbb{N}$. To confirm this, we examine the resonant wavelengths of the horizontal cavity for a range of diameters, wavelengths (1.3 and 0.91 μm), and background materials (air and BCB). In figure 2(i) this has been plotted and shows the independence of the side modes from the background index, and that for the 5–10 λ/n range (corresponding to diameter 1.5–3.0 μm) it is sufficiently accurate for use as a predictive tool. For larger diameters, a full 2D treatment of the resonator using Bessel functions would be necessary for accuracy. This shows as expected an increased suppression for the higher refractive index material (GaAs/air) providing a stronger suppression and increased enhancement of Γ_{Side} and overall wider variability comparing to the case that a dielectric has been used to planarize the micropillars.



4. Propagating Bloch modes

While the active coupling β quantifies the probability of Purcell enhanced decay into the cavity, it does not differentiate between emission vertically upwards or downwards. In order to get the full picture, we also need to examine the passive efficiency η (as calculated in equation (3a)). The requirement to consider further factors is illustrated in the devices discussed in figures 2(f) and (g) where despite the 2.95 μm and 3.00 μm pillar having similar β factors (0.68 and 0.72, respectively), differences in the passive efficiency η (0.73 and 0.79) lead to more strongly contrasting efficiencies ξ (0.50 and 0.57). A result of increased leakage into the substrate, this efficiency-reducing effect had been observed in analysis of narrow micropillar structures [20], with analogous effects attributed to Fabry–Perot modes in photonic crystals preventing near-ideal photon



extraction [21]. A detailed analytical treatment in agreement with experimental measurements [22] had followed shortly, where it was identified that modes exist whose effective index is solely real, resulting in no Bragg reflection and unrestricted propagation through the micropillar structure. It was further shown in [22] that the well-guided cavity mode Γ_{Cavity} can scatter at a reflective interface and excite propagating Bloch modes, with the energy leakage rate proportional to the scattering strength of the interface (i.e. reflected field intensity) as well as the spatial mode overlap at said interface. An example of a micropillar with strong leaky Bloch modes is presented in figure 3(a), showing the Fourier transform of $E(t)$ in a plane going through the pillar middle. The colormap is scaled to highlight the propagating Bloch modes which propagate through the structure; this particular micropillar has 7/35.5 top and bottom DBR pairs and a $2.25 \mu\text{m}$ diameter; the highly reflective GaAs-air interface at the micropillar top occurs at a point of significant spatial overlap between lower- and higher-order Bloch modes. This leads to significant excitation of the Bloch modes, leading to the observed η factor reduction. In this section, we explore the dependence of the Bloch mode resonant wavelengths on the diameter d_{Cavity} and the top and bottom DBR stack lengths, which is controlled by $N_{\text{Top}}, N_{\text{Bottom}}$, demonstrating the crucial need to spectrally detune the lossy propagating Bloch modes from the cavity mode and use off-resonant Purcell suppression to minimise any Γ_{Bottom} leakage. However, unlike the β factor and the singular Γ_{Side} mode and its harmonics, the peaks in Γ_{Bottom} are comprised of a plurality of repeated modes as exemplified in figure 3(b), and a detuning strategy is not as straightforward.

The need to expand our design strategy past the side loss minimising vertical-and-horizontal resonant cavity model is evident in the plot of the peak/on resonance efficiency factors as a function of d_{Cavity} in figure 3(c), where we observe variations in the η factor which are independent of the β factor ones and cause some full wavelength diameters to be much more efficient, i.e. have a higher ξ than others. In figure 3(d), we show the wavelength-resolved decay into the substrate, Γ_{Bottom} , as a function of the diameter where the absence of Γ_{Cavity} contributions signals that the well guided modes of the cavity are reflected upward by the

35.5 DBR pairs in the bottom stack, while one can identify a variety of low and high Q modes whose resonant wavelength is affected by d_{Cavity} . As a result of Γ_{Bottom} enhancement, it can be seen from the heatmap in figure 3(e) of η as a function of wavelength and diameter that the passive efficiency is high when the cavity mode dominates and diminished when Γ_{Bottom} is spectrally degenerate.

Plots of the on-resonance passive efficiency of the 2.25 μm pillars (with air as the background medium) with 15.5, 20.5, and 35.5 bottom DBR pairs have been shown in figure 3(f) as a function of the top DBR pairs. An initial increase in η , due to the strengthening Purcell factor F_p , is interrupted by a dip caused by strong Bloch mode at $N_{\text{Top}} = 7$, regardless of N_{Bottom} as the mode overlap is determined by the diameter and the path length between the emitter and the topmost interface. Further additions of DBR pairs in the top mirror tune the problematic mode away once more, recovering the high passive efficiency if the cavity remains single-sided. If there are not sufficient pairs in the bottom mirror, the increased reflectivity in the top directs the cavity mode itself into the substrate. A 1D estimation of the ratio of the Fresnel transmission coefficients $T_{\text{Top}}/T_{\text{Bottom}}$, calculated using the Transfer Matrix Method (TMM), is shown in figure 3(g). The blue region marks micropillars where the top/bottom DBR configuration cavities where most of the emission exits from the top, whereas pink denotes cavities where the emission is directed downward into the substrate by the overly high reflectivity of the top DBR, and a white dashed line serves as a visual guide to the ‘turning’ point where further top mirrors start to cause avoidable η losses. It can be seen that even for a modest amount of top pairs, $N_{\text{Bottom}} \geq 30.5$ is needed to optimise the micropillar.

5. Photon-phonon inhibition

It has long been predicted that the presence of a narrow bandwidth cavity with a significant Purcell enhancement on resonance will reduce coupling to phonon modes by ensuring that the rate of coupling on-resonance to the zero-photon line (ZPL) dominates over emission into the off-resonant phonon sideband (PSB) which extends several meV away from the ZPL even at 0 K. However there has been some debate as to whether the Purcell factor required to suppress the PSB to desirable levels means approaching the strong coupling regime [23]. We find here that the situation becomes more promising when moving away from the atomic approximation. As we have discussed, away from resonance from the cavity, a weak but important Purcell suppression is observed. As well as reducing decay into undesirable spatial channels, Purcell suppression can be used to reduce the available density of states of the PSB. In contrast to the atomic-like cavity approximation, the micropillar *suppresses* a significant fraction of the PSB due to the significant off-resonant Purcell suppression reducing the off resonant density of states. This is in contrast to the predicted effect of the cavity acting as a passive spectral filter, which simply reduces the overall efficiency.

We quantitatively examine whether the concurrent strengthening of the ZPL and weakening of the PSB field components can be used to near-eliminate any dephasing due to phonon side band emission by firstly considering the spectrum of the emitted field in bulk GaAs by a QD on resonance with the cavity and linewidth $\hbar\Gamma_0 = 0.5 \mu\text{eV}$ as an estimate, which has been shown in figure 4(a). The spectrum $S_{\text{Bulk}}(\omega)$ consists of a narrow ZPL Lorentzian and a broadband PSB such that the ZPL weight over $4\pi \text{ sr}$ is calculated as

$$W_{4\pi} = \frac{\int_{-\infty}^{\infty} S_{\text{ZPL}}(\omega) d\omega}{\int_{-\infty}^{\infty} S_{\text{Bulk}}(\omega) d\omega} \quad (5)$$

where S_{ZPL} is the ZPL portion of the field spectrum. We model the PSB phenomenologically, such that $W_{4\pi} = 90\%$, which errs on the pessimistic side of experimental measurements and theoretical models, where at 4 K $W_{4\pi}$ is in the 90%–93% range [23–29]. This remaining 10% of the spectrum arises from emission via the phonon density of states, $D_{\text{Ph}}(\omega, T)$ (figure 4(b)), which depends on the vertical and lateral sizes of the ground and excited electron wave functions $L_{i,j}$ where $i \in \{e, g\}$, $j \in \{xy, z\}$, where we use the analytical and experimental models presented in [30, 31],

$$D_{\text{PH}}(\omega, T) = \frac{\hbar}{4\pi d c_l^5} \frac{\omega^3}{1 - e^{-\frac{\hbar\omega}{k_B T}}} \int_0^1 (D_e e^{\tilde{\omega}_{e,xy}^2(u^2-1) - \tilde{\omega}_{e,z}^2 u^2} - D_g e^{\tilde{\omega}_{g,xy}^2(u^2-1) - \tilde{\omega}_{g,z}^2 u^2}) du \quad (6)$$

where $\tilde{\omega}_{i,j} = \omega L_{i,j}/(2c_l)$, with deformation potentials $D_e = -14.6 \text{ eV}$ and $D_g = -4.8 \text{ eV}$, and crystal density $d = 5370 \text{ kg m}^{-3}$. The characteristic wavefunction lengths have also been taken from roughly 0.95 μm dots measured in [30]; as the electron wavefunctions for O-band QDs will likely be larger, which leads to weaker photon-phonon dephasing [26], we are slightly overestimating the phonon contributions to the emitted spectrum and any ZPL weights calculated in this manner represent a lower bound; in reality the phonon sideband could contribute even less. The field spectrum S_{Bulk} is then acted upon by the FDTD-calculated cavity. An example of the 13/35.5 $5\lambda/n$ pillar modified emission has been plotted in figure 5(c) (blue line),

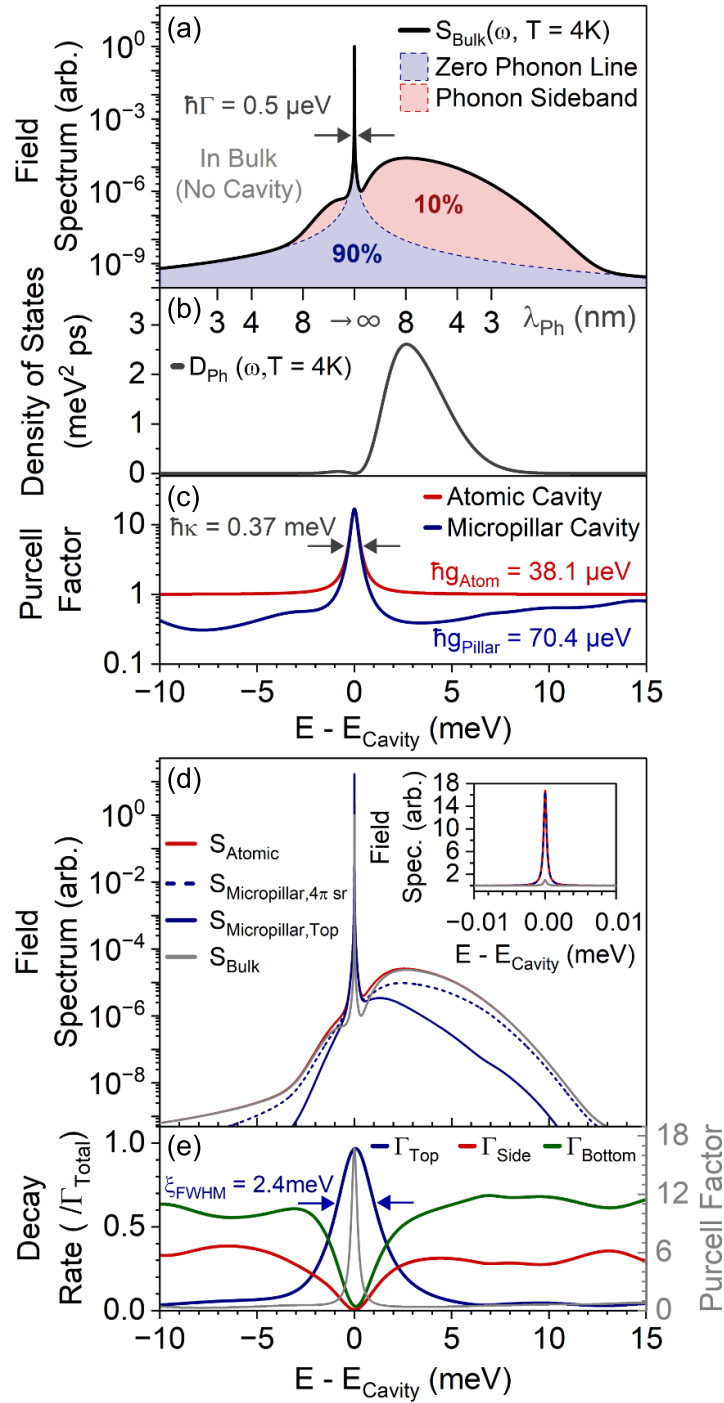


Figure 4. (a) A simulated field QD emission spectrum in bulk GaAs (without any cavity Purcell effects) with a ZPL weight of 90%. (b) The phonon density of states D_{Ph} at 4 K (7) generates the phonon sideband in the field spectrum, where we highlight the zero phonon density at exact resonance and the phonon absorption peak several meV away. (c) The FDTD-calculated Purcell factor of the 13/35.5 micropillar cavity (blue) shows off-resonant suppression of photon-phonon interactions as $\Gamma_{\text{Side}} < \Gamma_0$ at large $E - E_{\text{Cavity}}$, whereas an equivalent atomic emitter would not. (d) The spectra of the QD emitted field over 4π sr in bulk GaAs (grey), where there is no Purcell effect, is compared to that of an atom-like cavity (red), where only Purcell enhancement is modeled, and to the field emitted in an FDTD simulated micropillar cavity (dashed, blue), where off-resonant suppression of the PSB is also included. The solid blue line shows the field collected through the micropillar top. (e) The decay rates through the micropillar faces, normalised to the total power emitted. The suppression of undesired decay channels close to resonance with the cavity leads to a much wider efficiency FWHM (ξ_{FWHM}) i.e. the width of $\Gamma_{\text{Top}}/\Gamma_0$ in blue ($= \xi$) is several-fold broader than the width κ of the Purcell factor (grey, right axis).

which is compared to the effects of a similar structure with the atomic cavity approximation, which gives the same peak and FWHM, but a constant $F_{\text{P}} \rightarrow 1$ at large detuning. It is worth noting that because the actual micropillar cavity goes to $F_{\text{P}} \rightarrow 0.3$, the base-to-peak contrast is much larger than in the atomic case. The suppression of alternative decay leads to stronger coupling as a Lorentzian peak-to-base ratio of ≈ 55 , where

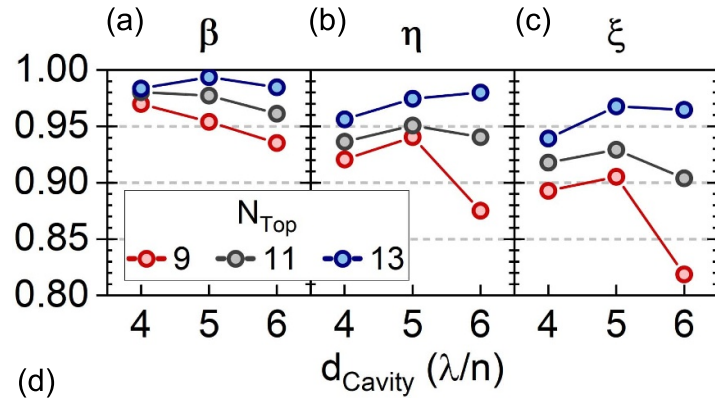


Figure 5. (a)–(c) The efficiency factors of micropillars: (a) emitter cavity coupling β , (b) passive optical efficiency of the cavity η , (c) efficiency out of the micropillar top $\xi = \beta\eta$, at full wavelength diameters, with $N_{\text{Bottom}} = 35.5$ and increasing N_{Top} . We choose an optimal $d_{\text{Cavity}} = 5\lambda/n$ for the figures in the table below. (d) figures of merit for high-efficiency low Q micropillars with $N_{\text{Bottom}} = 35.5$ DBR pairs and pillar diameter $d_{\text{Cavity}} = 5\lambda/n_{\text{Cavity}}$. Losses due to the PSB being redirected into the sides by the collection ‘filter’ ξ are quantified in ξ_{Phonon} , while the device efficiency $\epsilon = \xi \xi_{\text{Phonon}}$ describes the device efficiency when both structural and PSB-mediated losses are accounted for. The purity values for the resonant two-level system (2LS) and the biexciton pumping scheme are extrapolated from [5]. The final row $\epsilon\mathcal{I}$, describes the probability of an excitation pulse resulting in an indistinguishable photon being emitted from the top of the pillar.

the Purcell factor as a function of detuning is given by

$$F_P = \frac{\Gamma_{\text{Total}}}{\Gamma_0} = \Gamma_0 \left(1 + 2 \frac{g^2}{\kappa \Gamma_0} \frac{\frac{\kappa}{2}}{\left(\frac{\kappa}{2}\right)^2 + \Delta^2} \right) \quad (7)$$

where Δ is the atom-cavity detuning $\omega_{\text{Cavity}} - \omega_{\text{Emitter}}$ [16], we find that in order to keep a consistent peak-to-base ratio, $\hbar g_{\text{Pillar}} = 70.4 \mu\text{eV}$, while $\hbar g_{\text{Atom}} = 38.1 \mu\text{eV}$; this stronger coupling to the cavity further weakens the dephasing due to phonons [32]. The off-resonant Purcell suppression of the field spectrum, as

well as the cavity enhancement of decay into the ZPL work simultaneously to bring up the ZPL weight of the detected field (assuming the detector collects only Γ_{Top}) from $W_{4\pi} > 98\%$ to $W_{\text{Top}} > 99\%$. We model field-spectra by considering the bulk field enhanced in either an atom-like or micropillar cavity over the entire space, $S_{4\pi}$, and the field which would be collected through the top surface, S_{Top} , such that

$$S_{4\pi}(\omega) = F_P S_{\text{Bulk}}(\omega) \quad (8a)$$

$$S_{\text{Top}}(\omega) = \xi F_P S_{\text{Bulk}}(\omega). \quad (8b)$$

The spectra shown in figure 4(d), show the enhancement of the ZPL provided by both atomic-like and realistic micropillar cavities in the inset, where the actual micropillar cavity allows for off resonant suppression, resulting in $30\times$ suppression of the PSB relative to the ZPL. We note a subtlety that affects the efficiency out the top ξ versus detuning from the cavity; the efficiency drops off much more slowly than the Purcell factor (see grey vs. blue plots in figure 4(e)) due to off resonant suppression of lossy channels. Previous works have used the cavity decay rate κ as a spectral filter width [23, 26], whereas the much broader ξ function is a more accurate calculation of the photonic losses as it includes the reduction of leaky decay as $E - E_{\text{Cavity}} \rightarrow 0$. The bandwidth of ξ is an order of magnitude larger than κ , allowing for significantly shorter excitations pulses to reach the QD, leading to much higher purity as discussed in the next section.

6. Efficient pillar designs and discussion

After dealing with the major source of losses (side leakage and Bloch modes) and also considering the suppression of the PSB, we are now in a position to propose micropillar designs that simultaneously meet the requirements of (i) very high overall efficiency (ii) very low emission into the phonon sideband and (iii) broad cavities allowing for the input of ultrafast pulses, something we discuss quantitatively later in this section. We scan for optimal pillars across several optimal full wavelength diameters d_{Cavity} , as we showed in figure 2 that these will result in the strongest side loss suppression. Selecting $N_{\text{Bottom}} = 35.5$ ensures a strong emission out of the top of the pillar and $N_{\text{Top}} \in \{9, 10, 11\}$ results in Purcell enhanced yet sufficiently broadband cavities. It was demonstrated in figure 3(c) that the effects of propagating Bloch modes cannot be ignored when choosing the best device diameter. To closely examine this, the on-resonance peak values of the active coupling β , passive efficiency η , and the internal (at first lens) efficiency ξ of the cavity are presented in figures 5(a)–(c). Following only these two simple principles from sections 3 and 4, we have reduced the parameter space of the d_{Cavity} , N_{Top} , and N_{Bottom} optimisation problem from a 3 dimensional space to a few points, and we present designs which all but eliminate the side losses ($\beta = 99\%$ of the $13/35.5$ pillar at $5\lambda/n$ diameter). In examining Bloch mode losses, we note a substantial increase in the η factor of the $6\lambda/n$ diameter pillars in figure 5(b) when N_{Top} is incremented from 9 to 13 pairs. This is the result of a Γ_{Bottom} propagating Bloch mode being tuned away from the cavity. It is imperative to minimise any spectral overlap, and the $5\lambda/n$ diameter seems the most suitable choice as large changes in N_{Top} result in minimal η -changes and conversely, $6\lambda/n$ is unsuitable. We have therefore 3 high performing pillars with $N_{\text{Bottom}} = 35.5$, $N_{\text{Top}} = \{9, 11, 13\}$ and efficiency $\xi = \{0.905, 0.929, 0.966\}$, with respective cavity FWHM of $\approx \{1.31, 0.69, 0.37\}$ meV. In figures 5(a)–(c) we demonstrate that by including the full 3D effects of the micropillar structure, the internal efficiency extends well beyond the atomic-like cavity predictions and much closer to near-unity efficiency than previously thought, with each of the 3 designs having $\xi > 90\%$ of emitted photons exiting through the top of the micropillar.

Having identified good micropillar designs, we present their figures of merit in figure 5(d). The on-resonant values include standard cQED parameters, such as the cavity linewidth κ , the Purcell factor F_P , and the Q factor, as well as the efficiency factors of the cavity. We also report phonon-mediated losses to be at least an order of magnitude lower than in bulk. We consider that the photonic structure partially redirects the off-resonant PSB out of the cavity by introducing a phonon-adjusted device efficiency ϵ such that

$$\epsilon = \frac{\int_{-\infty}^{\infty} S_{\text{Top}}(\omega) d\omega}{\int_{-\infty}^{\infty} S_{4\pi}(\omega) d\omega} \equiv \xi \xi_{\text{Phonon}} \quad (9)$$

where ξ quantifies the losses due to the photonic structure, while ξ_{Phonon} quantifies the phonon-mediated losses due to the lower efficiency at the PSB peak a few meV off resonance. As such, the device efficiency ϵ accounts for the PSB whereas the FDTD-obtained ξ does not. To determine the impact of phonon dephasing on the indistinguishability, we assume that all other dephasing contributions are negligible and we estimate an expected indistinguishability

$$\mathcal{I} = W_{\text{Top}}^2 \quad (10)$$

which captures the indistinguishability limitations solely due to PSB dephasing, but does not take into account contributions from sources other than the PSB; a polaron frame treatment would be needed to include the effects of coherent QD-phonon interactions. In reality, the non-Markovian interactions of the electron spin with the nuclear spin bath of the solid state QDs [33, 34] will have a meaningful contribution which has not been captured by equation (10), but this is an obstacle which is independent of the cavity-emitter interactions discussed in this work. Nevertheless, when analysing the effect of phonon dephasing it can still be said that despite being low Q , due to the near-elimination of the phonon sideband we report high expected indistinguishabilities of $\approx 98.5\%$ – 99.84% , with spectrally stronger cavities giving better values for $\epsilon\mathcal{I}$, albeit at the cost of a narrower bandwidth photonic structure. As such, the most suitable design depends on the requirements, and the pillars presented can fulfil different roles: for instance, a lower overall efficiency but broad micropillar (9/35.5) is more favourable for collection of a biexciton-exciton pair, whereas a more narrowband pillar with a higher efficiency (13/35.5) is better suited for efficient generation of high fidelity linear cluster states, as the chance of successfully extracting an indistinguishable photon given by $\epsilon\mathcal{I} = 0.9625$, the probability of generating a 16-qubit chain is given by $(\epsilon\mathcal{I})^{16} = 0.9625^{16} \approx 54\%$. The 13/35.5 design is also suitable for applications such as boson sampling, where reasonable efficiency $>50\%$ and very high indistinguishability is required, or for use as a light-matter interface in non-linear interactions as a switch or a quantum memory.

As well as photon extraction efficiency and indistinguishability, the third parameter to consider is the single photon purity, i.e. the suppression of multiphoton events, usually parameterised by $g^{(2)}(0)$. Previous research has shown how the $g^{(2)}(0)$ scales with excitation pulse length [5]: when resonantly exciting a 2LS with temporally increasingly longer pulses the probability of decay and re-excitation within the pulse time increases. The situation improves when a two-photon excitation of a biexciton state (three level XX-X cascade) is used as two photons must be emitted before excitation. This fact does impose limits on the bandwidth of the cavity: broader cavities can accommodate shorter pulses. We find that due to the off-resonant Purcell suppression, the efficiency width ξ_{FWHM} is much broader than the cavity Q factor. Taking ξ_{FWHM} as a limit on the maximum pump pulse width, or rather the minimal pulse length permitted by the structure, we get pulse lengths of 0.9, 1.4, and 1.7 ps for the 9, 11, and 13 top pair pillars discussed in figure 5. Assuming that the lifetime of a QD in bulk semiconductor is $T_1 = 1$ ns, the shortest pulses which fit inside the three micropillars highlighted in figure 5 correspond to only ~ 0.001 of the dot lifetime, and following the rationale and theoretical framework discussed in [5] (see figure 3(a) of that article), we predict $g^{(2)}(0)$ values of order of magnitude $\sim 10^{-3}$ for a resonantly excited 2LS, and $\sim 10^{-5}$ for a biexciton pumping scheme (see table for exact values). This shows that due to the high efficiency ‘bandwidth’ resulting from the low Q resonance combined with off-resonant suppression, these structures can result in $>99.3\%$ single photon purity for the resonantly excited 2LS, or $>99.99\%$ if a pillar is broad enough to allow for a biexciton excitation scheme.

While the device efficiency ϵ represents the brightness out of the top of the pillar, the far field angular distribution of the emitted mode and the corresponding collection efficiency within some NA have been unaddressed in this work. Many of the figures of merit presented here may be improved by various means. Overall extraction efficiencies may be tuned by, for example, introducing adiabatically varying DBR layers and controlling the refractive index contrast of the final top layer of material, and there is similar scope for engineering the Bloch modes to be minimal. Reduction of the coupling to phonon modes may be controlled further by controlling the QD growth or material. We also note that many practical issues still remain to be resolved, some of which are known, spectral wander from charge noise for example, or an examination of fabrication tolerances and deviations from our simple design. Practical realisation of QD photonic structures with such figures of merit will likely reveal other unanticipated sources of loss and distinguishability, however, we believe that the demonstration of micropillar designs with $\geq 95\%$ overall single photon emission efficiency and suppression of the phonon coupling to give indistinguishabilities of $\geq 99.9\%$ in some cases paves the way for an engineering approach to reaching even higher values, and demonstrate that there are no fundamental roadblocks to achieving QD sources for the most demanding high end applications. The scope of application of highly efficient and indistinguishable sources goes beyond low-fault quantum computing, such as quantum repeaters in quantum networks [35, 36]; another use would be to use the broader 9/35.5 micropillar to simultaneously efficiently extract a spin entangled biexciton-exciton photon pair which could be used for device independent quantum cryptography [37, 38], or alongside quantum memories to do remote quantum teleportation of states, a necessary element of the quantum internet [39, 40].

7. Conclusion

We demonstrate in this work designs for plain micropillar structures using industry standard techniques with record-breaking efficiency in the weak coupling Purcell regime. We achieve simultaneously in one

device design overall single photon extraction efficiency of $\xi > 96\%$, phonon sideband suppression that should yield photon indistinguishabilities of $\mathcal{I} > 99.9\%$ in a $Q = 2500$, which is low enough to allow optical coherent control pulses of a few ps while also providing increased resistance to fabrication imperfections such as sidewall roughness or asymmetry which can prevent polarization degenerate emission. While design of outcoupling strategies goes beyond the scope of this work, we believe our cavity design strategy demonstrates the plausibility of broadband micropillars which are comparatively easier to manufacture than high Q structures demanding more DBR pairs and more durable than similar structures with equivalent efficiencies such as nanotrumpets, nanowires, or hourglass micropillars, but can still operate as near-perfect on-demand sources of indistinguishable photons and deterministic non-linearities for even the most demanding applications, such as fault-tolerant photonic quantum computing. It is important to mention that some of the underlying assumptions, such as the QD-Cavity spectral overlap and the spatial positioning of the emitter in cavity center still require non trivial fabrication. We emphasise that the figures of merit presented do not represent a theoretical limit, and we anticipate that with careful engineering even higher efficiencies and phonon suppression can be designed. Our designs can also be applied to a wide range of target wavelengths. Moreover, the principles applied to these QD micropillar cavities, i.e. careful consideration of the photonic density of states in all three dimensions, careful understanding of how the cavity can modify the phononic modes, can be applied to other photonic structures. For instance, photonic crystal waveguides could be modified to include low Q factor adiabatic cavities which would better control the phonon sideband. Likewise, similar Bloch-like leaky modes may appear in bullseye structures, and careful engineering of the phononic density of states with the cavity will be important for other emitters such as colour centres in diamond and SiC.

Data availability statement

The data cannot be made publicly available upon publication because no suitable repository exists for hosting data in this field of study. The data that support the findings of this study are available upon reasonable request from the authors.

Acknowledgments

The authors would like to acknowledge contributions and useful discussions from Sam Mister and Asciah M S Alshahrani.

Funding

This project has benefited from funding by EPSRC Grant EP/N003381/1, and from the Ministry of Education and Science of the Republic of North Macedonia. PA acknowledges financial support provided by EPSRC via Grant No. EP/T001062/1.

ORCID iD

D Dlaka  <https://orcid.org/0000-0002-7579-7646>

References

- [1] Somaschi N *et al* 2016 *Nat. Photon.* **10** 340–5
- [2] Ding X *et al* 2016 *Phys. Rev. Lett.* **116** 020401
- [3] Unsleber S, He Y M, Gerhardt S, Maier S, Lu C Y, Pan J W, Gregersen N, Kamp M and Schneider C 2016 *Opt. Express* **24** 8539
- [4] Tomm N *et al* 2021 *Nat. Nanotechnol.* **16** 399–403
- [5] Hanschke L, Fischer K A, Appel S, Lukin D, Wierzbowski J, Sun S, Trivedi R, Vučković J, Finley J J and Müller K 2018 *npj Quantum Inf.* **4** 43
- [6] Androvitsaneas P *et al* 2023 *Appl. Phys. Lett.* **123** 094001
- [7] Androvitsaneas P *et al* 2016 *Phys. Rev. B* **93** 241409(R)
- [8] Androvitsaneas P *et al* 2019 *ACS Photon.* **6** 429–35
- [9] Ginés L *et al* 2022 *Phys. Rev. Lett.* **129** 033601
- [10] Munsch M, Malik N S, Dupuy E, Delga A, Bleuse J, Gérard J M, Claudon J, Gregersen N and Mørk J 2013 *Phys. Rev. Lett.* **110** 177402
- [11] Osterkryger A D, Claudon J, Gérard J M and Gregersen N 2019 *Opt. Lett.* **44** 2617
- [12] Gaál B, Jacobsen M A, Vannucci L, Claudon J, Gérard J M and Gregersen N 2022 *Appl. Phys. Lett.* **121** 170501
- [13] Wang H *et al* 2019 *Nat. Photon.* **13** 770–5
- [14] Gür U M, Mattes M, Arslanagić S and Gregersen N 2021 *Appl. Phys. Lett.* **118** 061101
- [15] Reitzenstein S and Forchel A 2010 *J. Phys. D: Appl. Phys.* **43** 033001
- [16] Carmichael H J 2009 *Statistical Methods in Quantum Optics 2* (Springer Science & Business Media)
- [17] Wang B Y, Häyrynen T, Vannucci L, Jacobsen M A, Lu C Y and Gregersen N 2021 *Appl. Phys. Lett.* **118** 114003

- [18] Jacobsen M A, Wang Y, Vannucci L, Claudon J, Gérard J M and Gregersen N 2023 *Nanoscale* **15** 6156–69
- [19] Ismail N, Kores C C, Geskus D and Pollnau M 2016 *Opt. Express* **24** 16366
- [20] Lalanne P, Hugonin J P and Gérard J M 2004 *Appl. Phys. Lett.* **84** 4726–8
- [21] Rigal B, Dwir B, Rudra A, Kulkova I, Lyasota A and Kapon E 2018 *Appl. Phys. Lett.* **112** 051105
- [22] Lecamp G, Lalanne P, Hugonin J P and Gérard J M 2005 *IEEE J. Quantum Electron.* **41** 1323–9
- [23] Iles-Smith J, McCutcheon D P, Nazir A and Mørk J 2017 *Nat. Photon.* **11** 521–6
- [24] Borri P, Langbein W, Schneider S, Woggon U, Sellin R, Ouyang D and Bimberg D 2001 *Phys. Rev. Lett.* **87** 157401
- [25] Muljarov E A and Zimmermann R 2004 *Phys. Rev. Lett.* **93** 237401
- [26] Denning E V, Iles-Smith J, Gregersen N and Mørk J 2019 *Opt. Mater. Express* **10** 222–36
- [27] Borri P, Langbein W W, Woggon U, Schwab M, Bayer M, Fafard S, Wasilewski Z R and Hawrylak P 2003 *Phys. Rev. Lett.* **91** 267401
- [28] Borri P, Langbein W, Woggon U, Stavarache V, Reuter D and Wieck A D 2005 *Phys. Rev. B* **71** 115328
- [29] Bommer M, Schulz W M, Roßbach R, Jetter M, Michler P, Thomay T, Leitenstorfer A and Bratschitsch R 2011 *J. Appl. Phys.* **110** 063108
- [30] Madsen K R, Kaer P, Kreiner-Møller A, Stobbe S, Nysteen A, Mørk J and Lodahl P 2013 *Phys. Rev. B* **88** 045316
- [31] Kaer P, Nielsen T R, Lodahl P, Jauho A P and Mørk J 2012 *Phys. Rev. B* **86** 085302
- [32] Kaer P, Lodahl P, Jauho A P and Mørk J 2013 *Phys. Rev. B* **87** 081308
- [33] Cywinski L, Witzel W and Sarma S D 2009 *Phys. Rev. Lett.* **102** 057601
- [34] Cywiński L 2011 *Acta Phys. Pol. A* **119**
- [35] Azuma K, Economou S E, Elkouss D, Hilaire P, Jiang L, Lo H K and Tzitrin I 2023 *Rev. Mod. Phys.* **95** 045006
- [36] Muralidharan S, Li L, Kim J, Lütkenhaus N, Lukin M D and Jiang L 2016 *Sci. Rep.* **6** 20463
- [37] Pironio S, Acín A, Brunner N, Gisin N, Massar S and Scarani V 2009 *New J. Phys.* **11** 045021
- [38] Vazirani U and Vidick T 2019 *Commun. ACM* **62** 133
- [39] Kimble H J 2008 *Nature* **453** 1023–30
- [40] Orioux A, Versteegh M A M, Jöns K D and Ducci S 2017 *Rep. Prog. Phys.* **80** 076001